HHS Public Access

Author manuscript

Life Sci. Author manuscript; available in PMC 2024 January 01.

Published in final edited form as:

Life Sci. 2023 January 01; 312: 121128. doi:10.1016/j.lfs.2022.121128.

CircRAD54L2 promotes triple-negative breast cancer progression by regulating the miR-888 family/PDK1 axis

Qiancheng He[1,*], **Qiongyu Hao**[2,*], **Yanyuan Wu**[2,3], **Jaydutt V. Vadgama**[2,3,#], **Yiyan Jiang**[4,#]

[1.]Department of General Medicine, The First Affiliated Hospital of Wenzhou Medical University, Wenzhou, Zhejiang 325000, China.

[2.]Department of Internal Medicine, Charles Drew University of Medicine and Science, Los Angeles, CA 90059, USA.

[3.]Jonsson Comprehensive Cancer Center, David Geffen School of Medicine, University of California at Los Angeles, Los Angeles, CA 90095, USA.

[4.]Department of Oncology, The First Affiliated Hospital of Wenzhou Medical University, Wenzhou, Zhejiang 325000, China.

Abstract

Background: The long-term prognosis of breast cancer with metastasis remains extremely poor. Genetic alterations in tumor cells result in cellular heterogeneity, promoting cancer cells invasion and colonization in some organs during the metastatic process. CircRNAs are very promising as critical biological markers and precise diagnoses in identifying disease mechanisms and developing new methods for effective treatment. However, the role of aberrant expression of circRNAs in breast cancer progression remains largely unknown.

Methods: RNase R treatment and Quantitative RT-PCR (qRT-PCR) were performed for circRNA detection. Transwell chamber assays were used to examine the chemotactic migration and invasion of breast cancer cells.

Results: This study identified and characterized the circRAD54L2 originating from exon 1, 2, 3, and 4 of the RAD54L2 gene. Importantly, we found that circRAD54L2, rather than RAD54L2

[#]Corresponding authors: Jaydutt V. Vadgama, Ph.D., 1731 E. 120th St. Los Angeles, CA 90059, USA. jayvadgama@cdrewu.edu; Yiyan Jiang, M.D., Ph.D., 2 Fuxuexiang, Wenzhou, Zhejiang 325000, China. jiangyiyan@wzhospital.cn.

[*]Co-first authors:
Qiancheng He and Qiongyu Hao contributed equally as co-first authors.

Authors' contributions

Study concept and design: Y.J.; Acquisition of data: Q. He and Q. Hao; Analysis and interpretation of data: Q. He and Q. Hao; Drafting of the manuscript: Q. He; Critical revision of the manuscript: Y. Jiang; funding acquisition: Y. Jiang, Q. Hao, Y.Wu, and J.V.Vadgama.

Ethical Approval and Consent to participate:
Yes.

Consent for publication:
Yes.

Availability of data and materials:
Yes.

Competing interests:
The authors declared that they do not have anything to disclose regarding funding or conflict of interest in this manuscript.

linear mRNA, was significantly upregulated in breast cancer cell lines. Furthermore, we found that inhibiting circRAD54L2 expression markedly reduced the invasion, metastasis, and proliferation of breast cancer cells via sponging of the miR-888 family, which downregulated the expression of pyruvate dehydrogenase kinase 1 (PDK1).

Conclusion: Our results showed that circRAD54L2 could regulate PDK1 expression by sponging the miR-888 family competing for the ceRNA mechanism, indicating that circRAD54L2 may act as an essential upstream regulator and providing further mechanistic evidence to support the notion that circRAD54L2/miR-888s/PDK1 is a promising therapeutic target in the treatment of breast cancer.

Keywords

TNBC; CircRNAs; MicroRNA; miR-888; PDK1

Introduction

Breast cancer is the most common cancer diagnosed in women, accounting for more than 1 in 10 new cancer diagnoses each year. It is the second most common cause of death from cancer among women [1]. Global gene expression profiling studies classified breast cancer into five intrinsic subtypes by hierarchical clustering, namely luminal A, luminal B, HER2-overexpressing, basal-like breast cancer (BLBC), and normal-like tumors [2]. The BLBC lacks ER, PR, and HER2-related gene expression and shows a triple-negative phenotype (TNBC). Histologically, TNBC is usually a high grade with a high proliferation index. TNBC patients have a poor prognosis, and relapses may occur five years after diagnosis [3]. Thus, there is an urgent need to understand TNBC's molecular mechanisms better and identify novel therapeutic targets to improve clinical outcomes.

Circular RNAs (circRNAs) are a class of non-coding RNAs with a covalently closed loop structure that lacks 5'-3' polarity or a polyadenylated tail [4]. In the past decades, circRNAs have been identified in eukaryotic cells by electron microscopy and were previously considered as splicing error byproducts [5, 6]. With the development of deep RNA sequencing, many exonic and intronic circRNAs have been identified to be expressed in multiple cell lines and various species [7-9], indicating that circRNAs are not simply byproducts of splicing errors. Unlike linear RNAs, most circRNAs are formed by exon or intron back-splicing. Recent studies about circRNA biogenesis have revealed that some circRNAs play essential roles in cancer development [10, 11]. Some studies reported that circRNAs function as "miRNA sponges" by modulating their activity on other target genes, which play an inhibitory role in miRNA regulation [12, 13]. CircRNAs are very promising as critical biological markers and precise diagnoses in identifying disease mechanisms and developing new methods for effective treatment. However, the role of aberrant expression of circRNAs in breast cancer progression remains largely unknown.

Materials & methods

Identification of circRAD54L2 specific binding with miRNAs

The circRAD54L2 specific binding with miRNAs (hsa-miR-888, hsa-miR-890, and hsa-miR-892a/b) were identified using the Circular RNA Interactome database (https://circinteractome.nia.nih.gov/) in breast cancer cells [14]. The target genes of hsa-miR-888, hsa-miR-890, and hsa-miR-892a/b were screened using TargetScanHuman (http://www.targetscan.org/vert_72/) and miRDB (http://www.mirdb.org/).

Cell culture

Breast cancer cells lines MDA-MB-231 and MDA-MB-468 were initially obtained from the American Type Culture Collection (Rockville, MD) and applied for study within six months following resuscitation of frozen aliquots. All cells used in this study were tested for mycoplasma contamination and authenticated by short tandem repeat (STR) profiling. Cells were cultured in Leibovitz's L-15 Medium (Invitrogen, Grand Island, NY, USA) according to ATCC recommendation, supplemented with 10% FBS (Fetal Bovine Serum) (GIBCO, Brazil), penicillin (25 units/ml), streptomycin (25 g/ml), and 1% L-glutamine in an incubator with a humidified atmosphere of 5% CO_2 at 37 °C.

Transient transfection

Transfections were performed using the Lipofectamine 3000 kit (Invitrogen) according to the manufacturer’s instructions. The double-stranded microRNA mimics (Cat: MCH03911; Applied Biological Materials Inc.) at the 5'-end are designed, and chemically synthesized with a partially complementary motif to 3'UTR end of the target gene. It copies the functionality of mature endogenous miRNA upon transfection at a final concentration of 50 nM. The antisense single-stranded microRNA inhibitors (Cat: MIH03911; Applied Biological Materials Inc.) are chemically synthesized to target endogenous complementary mature miRNA upon transfection at a final concentration of 50 nM.

Knock down a circular RNA using shRNA

The sequence of the mature circular RNA often fully overlaps with that of its cognate linear mRNA, leaving the backsplicing junction as the only distinguishing (and thus targetable) feature in the mature circular RNA. Short hairpin RNA (shRNA) complementary to the backsplicing junction was used to deplete endogenous circRAD54L2. The shRNAs sequences for circRAD54L2 and control were listed in Table S2.

CircRNA *in vivo* precipitation (circRIP) and biotin-labeled miRNA capture

MDA-MB-231 and MDA-MB-468 cells seeded in 10-cm dishes were transfected with the specific biotin-tagged circRAD54L2 probe (Table S1) or biotin-labeled miR-888, miR-890, and miR-892a/b mimics at a final concentration of 200 nmol/L for 24 h. Streptavidin-Dynabeads (M-280, Invitrogen) were washed with lysis buffer; and blocked with yeast tRNA on a rotator at 4 °C for 2 h. The cells were fixed with 1% formaldehyde for 10 min when reaching sufficient confluency. Then the cells were lysed and sonicated. After centrifugation, cell lysis solution was incubated with the streptavidin-dynabead mixture

overnight at 4 °C. The mixture was washed and incubated in 200 μl lysis buffer with proteinase K. Finally, and total RNA was extracted using a miRNeasy Mini Kit according to the manufacturer's instructions. The abundance of circRAD54L2 and miR-888s in bound fractions was tested by qRT-PCR.

RNase R treatment and Real-Time Quantitative RT-PCR (qRT-PCR)

For circRNA detection, treatment with RNase R (3 U/mg, Epicentre Technologies, USA) was used to degrade linear mRNA. In brief, total RNA was split into two parts: one for RNase R digestion and the other for control with digestion buffer only. The samples were incubated at 37 °C for 30 min. Then the expression levels of circRAD54L2 were detected by quantitative real-time RT-PCR. Total RNA was isolated with the RNeasy Mini Kit (QIAGEN, Stockach, Germany). The cDNA was synthesized using a reverse transcription kit (Bio-Rad, Hercules, CA, USA). Quantification of mRNA and circular RNA was performed by using an SYBR Green PCR Kit (Bio-Rad, Hercules, CA, USA). Human 18s was selected as a housekeeping gene for mRNA and circRNA. The expression of miRNA was normalized to hsa-miR-26a-5p (477995_mir). TaqMan miRNA assays (Thermofisher Scientific, Waltham, MA, USA) were used to determine the miRNA level. All primers see Additional Table 1. Gene relative expression was calculated by the ΔΔCT method, where the fold enrichment was determined as $2^{-[\Delta CT\ (sample)\ -\ \Delta CT\ (calibrator)]}$.

Western blot analysis

Total proteins from the cells were extracted using a RIPA Lysis and Extraction Buffer (Thermo Scientific™, Cat#: 89900), including Halt™ Protease and Phosphatase Inhibitor Cocktail (100X) (Thermo Scientific™, Cat#: 78440). Lysates were denatured prior to sodium dodecyl sulfate-polyacrylamide gel electrophoresis (SDS-PAGE) and then transferred to polyvinylidene difluoride (PVDF) membranes (Millipore, Cat#: 3010040001). The membranes were blocked with 0.4% gelatin at room temperature for 1 h and then incubated with primary antibodies at 4 °C overnight. The membranes were washed and further incubated with secondary antibodies for 1 h the following day. The immunoreactive signals were visualized using chemiluminescence reagents SuperSignal™ West Femto Maximum Sensitivity Substrate (Thermo Scientific™, Cat#: 34094). Images were captured with the Odyssey® XF Imaging System (LI-COR Biosciences, U.S.). The following antibodies were used: PDK1 Antibody (Cell Signaling Technology, Cat#: 3062), α-Tubulin Antibody (Cell Signaling Technology, Cat#: 2144).

Cell viability

Cell viability was determined using the cell counting kit-8 (CCK8) (MilliporeSigma, Cat#: 96992). The cells were seeded in a 96-well plate at a density of ~5,000 per well. Cell viability was determined 48 h later. The cell medium was replaced with 100 μl of complete medium supplemented with 10 μl of CCK8, the cells were incubated in an incubator for 2 h. Absorbance values (OD) were measured at 450 nm in a GloMax®-Multi^{+} Detection System (Promega Corp, WI, USA).

Wound-healing assay

Cells were seeded in six-well plates and allowed to grow to confluence. The monolayer was scratched with a micropipette tip. The cells were cultured in a complete medium. The images of the wound area were captured at 0 and 24 h with a LEICA IRB microscope.

Cell migration assay and invasion assay

Chemotactic migration and invasion assay of MDA-MB-231 and MDA-MB-468 cells were examined with the Transwell Chamber Assay. Cells were seeded in a QCM 24-well Migration Assay plate (Sigma-Aldrich. Cat#: ECM508) and QCM Collagen Cell 24-well Invasion Assay plate (Sigma-Aldrich. Cat#: ECM551) with an 8μm pore size and colorimetric detection. The serum-free LEIBOVITZ'S L-15 medium was added in the upper inserts, and the complete LEIBOVITZ'S L-15 medium (containing 10% FBS) was added into the bottom chamber as a chemoattractant. After culture for 24-36 hours, non-migrating/invading cells on the membrane were removed by a swab, and migrated/invaded cells underneath the membrane were fixed with 4% formaldehyde and stained with crystal violet staining solutions according to the manufacturer's instructions. Migrated/invaded cell numbers were counted in five randomly selected fields under a microscope.

Luciferase reporter assays

Full length PDK1 3' UTR WT fragment and their corresponding mutation fragment at miR-888s binding sites were synthesized and cloned into the luciferase reporter vector psiCHECK-2, respectively. The sequence of UUUGAGU at seeding site was mutated with AAACUCA. All these plasmids were validated by sequencing. For reporter assays, WT or mutant reporter vector, psiCHECK-2-PDK1-3'-UTR-WT or MUT, were co-transfected with hsa-miR-888, miR-890, and miR-892a/b mimics, respectively, into MDA-MB-231 and MDA-MB-468 cells. The cells were lysed at 24 h after transfection and subjected to luciferase activity assays using the Dual-Glo system (Promega Corp, WI, USA).

Mouse model for experimental lung metastasis

All animal studies were conducted following the principles and procedures outlined in Guide for the Care and Use of Animals of The First Affiliated Hospital of Wenzhou Medical University. Mice were maintained on HEPA-filtered racks in a pathogen-free barrier facility and fed with an autoclaved laboratory rodent diet. MDA-MB-231 cells in 200 μl of medium containing 5% FBS were injected into mice via the tail vein for experimental metastasis. Histologic imaging analyses assessed pulmonary metastases on day 7 or 14 after tumor cell injection. For experiments monitoring extravasation, $\approx 1\times10^6$ MDA-MB-231 cells were incubated with XenoLight DiR dye for 1h at 37°C prior to the tail vein injection. The initial seeding in lungs, livers, and spleens was assessed by detecting XenoLight DiR–positive tumor cells using an IVIS Lumina II system. Isolated mouse lung lobes were washed with tris-buffered saline, fixed with paraformaldehyde, and sliced into sections of 4 mm thickness. Antigen-antibody complexes were labeled by avidin-biotinylated enzyme complex (ABC kit) and 3,3'-diaminobenzidine substrate kit after immunostaining with anti-Ki67 antibody. Then red alkaline phosphatase substrate kit (Vector Laboratories, Burlingame, CA) was applied for labeling α-SM actin after immunostaining with an anti-α-

SM actin-alkaline phosphatase antibody. Hematoxylin was used for counterstaining. Lung sections were visualized with a ZEISS AXIOPHOT microscope. A percentage of positive expressions of Ki-67 was calculated to assess the effects of circRAD54L2 on the *in vivo* metastasis of breast cancer cells.

Xenograft nude mouse model

To establish the subcutaneous xenograft *in vivo* model, ~5 x10^6 logarithmically growing circRAD54L2-overexpressing MDA-MB-231 cells or control parental cells in 0.1 ml Matrigel Matrix (Corning, Cat#: CB-40234) were subcutaneously injected into the left or right flank of 3-week-old male BALB/c nu/nu mice (n = 6). Mice were sacrificed, and tumor tissues were excised and weighed about 20 days later. The tumor volume was calculated using the equation: volume = width^2 ×length × 0.5 (mm^3).

Immunohistochemistry (IHC) assays

Tissues were fixed with 10% formalin and embedded in paraffin. Tissue sections were deparaffinized in xylene, rehydrated in a serial of graded ethanol, and antigens were retrieved by boiling in an antigen unmasking solution (Vector lab, Cat#: H-3301-250). Endogenous peroxidase activity was blocked with 10% goat serum for 30 min. The tissue sections were incubated with a primary antibody at 4 °C overnight and then with a secondary antibody for 1 h. The immunocomplexes were visualized with a 3,3′-diaminobenzidine tetrahydrochloride solution (DAB kit) (Vector lab, Catalog #: SK-4100), then the nucleus was stained with hematoxylin. Slides were covered by coverslips and sealed with a vectashield mounting medium (Vector lab, Catalog #: H-1500). The images were taken under MoticEasyScan Pro (Motic Digital Pathology, Fujian, China).

Lung histology staining

Isolated mouse lung lobes were washed with Tris-buffered saline, fixed with paraformaldehyde, and sliced into sections of 4 mm thickness. Antigen-antibody complexes were labeled by avidin-biotinylated enzyme complex (ABC kit) and 3,3’-diaminobenzidine substrate kit after immunostaining with anti-Ki67 antibody. Then red alkaline phosphatase substrate kit (Vector Laboratories, Burlingame, CA) was applied for labeling α-SM actin after immunostaining with an anti-α-SM actin-alkaline phosphatase antibody. Hematoxylin was used for counterstaining. Lung sections were visualized with a ZEISS AXIOPHOT microscope. A percentage of Ki67-positive cells was calculated to determine lung metastasis extent.

Statistical analysis

The data were expressed as the mean ± standard deviation (SD) of at least three independent experiments and were analyzed with Prism 6.0 software (GraphPad, San Diego, CA, USA). Statistical significance between two groups was analyzed using the Student’s t-test, while a multiple-group comparison was performed with a one-way analysis of variance (ANOVA). P-values less than 0.05 were considered statistically significant.

Results

CircRAD54L2 is upregulated in breast cancer cells.

Hsa_circ_0001306 has consisted of RAD54L2 exon 1-4 (Fig. 1A), referred to as circRAD54L2 hereafter, according to circBase. CircRAD54L2 showed a higher expression in 4 breast cancer cell lines (MDA-MB-231, MDA-MB-468, MCF7, and T47D) than in non-tumor breast cell line MCF-12A (Fig. 1B). The RNase-R assay showed that circRAD54L2 was relatively resistant to RNase-R and more stable than the linear mRNA of RAD54L2 in MDA-MB-231 and MDA-MB-468 cells (Fig. 1C, D).

Knockdown of circRAD54L2 inhibits proliferation and metastasis of breast cancer cells.

CircRAD54L2 knockdown lentiviral particles were transduced into MDA-MB-231 and MDA-MB-468 cells. Real-Time qRT-PCR analysis showed that circRAD54L2 was stably knocked down by sh-circRAD54L2 in MDA-MB-231 and MDA-MB-468 cells, and sh-circRAD54L2-#3 is the most effective (Fig. 2A). The MTS assay showed the cell viability was weakened in sh-circRAD54L2 transduced MDA-MB-231 and MDA-MB-468 cells (Fig. 2B). MDA-MB-231 cells that stably knockdown circRAD54L2 were injected into the dorsal subcutaneous tissues of 6 nude mice. Consistent with the *in vitro* findings, silencing of circRAD54L2 inhibited subcutaneous xenograft growth *in vivo* (Fig. 2C). The volumes of the tumors formed by circRAD54L2 knockdown MDA-MB-231 cells grew slower than in control mice (Fig. 2D). Taken together, these results reveal that silencing of circRAD54L2 inhibits the proliferation and tumorigenicity of TNBC cells.

Knockdown of circRAD54L2 inhibits breast cancer cell migration and invasion *in vitro* and tumor metastasis *in vivo*.

To investigate the correlation between circRAD54L2 and metastatic ability of breast cancer cells. Transwell migration and invasion assays were performed to assess the effect on migration and invasion in breast cancer cells. As expected, the migration and invasion capacity of both MDA-MB-231 and MDA-MB-468 cells were remarkably weakened by circRAD54L2 knockdown (Fig. 3A). The wound-healing assay also revealed that silencing of circRAD54L2 significantly inhibited TNBC cells migration (Fig. 3B). Subsequently, we found that the number and size of metastatic colonies in the lung were largely reduced by ectopic knockdown of circRAD54L2, which was confirmed by *in vivo* tail vein injection of MDA-MB-231 cells stably transduction with sh-circRAD54L2 in BALB/c nude mice model (Fig. 3C).

CircRAD54L2 abundantly sponges the miR-888 family members in breast cancer cells.

Given that circRNAs have been shown to function as a miRNA sponge, we next investigated the ability of circRAD54L2 to bind to miRNAs. Circular RNA Interactome (https://circinteractome.nia.nih.gov/) was used to predict the potential target miRNAs that could secure with the circRAD54L2 sequence. The miR-888 family was selected as the best possible target for circRAD54L2 (Fig. 4A). Next, circRAD54L2 was enriched on biotin-labeled hsa-miR-888, hsa-miR-890, hsa-miR-892a, and hsa-miR-892b using a miRNA pulldown assay in MDA-MB-231 and MDA-MB-468 cells (Fig. 4B, C, D, and

E). Reciprocally, a specific biotin-labeled circRAD54L2 probe was designed to perform RNA *in vivo* precipitation (RIP) to confirm whether the miR-888 family members can interact with circRAD54L2 in breast cancer cells. The results showed significant enrichment of hsa-miR-888, hsa-miR-890, hsa-miR-892a, and hsa-miR-892b circRAD54L2 compared to the controls (Supp. Fig. 1A, B, C, and D), indicating that circRAD54L2 sponged miR-888 family members in MDA-MB-231 and MDA-MB-468 cells. A luciferase reporter (Luc_circRAD54L2) was constructed by inserting the circRAD54L2 fragment into downstream of the luciferase gene. MiR-888 family members mimics and reporter genes were co-transfected into MDA-MB-231 and MDA-MB-468 cells. A notable reduction in luciferase reporter activity was observed when hsa-miR-888, hsa-miR-890, hsa-miR-892a, and hsa-miR-892b mimics co-transfection with wild-type luciferase reporter (Fig. 4F, G, H and I). Co-transfection with mutant luciferase reporter, miR-888 family member mimics did not change the luciferase reporter activity in MDA-MB-231 and MDA-MB-468 cells (Fig. 4F, G, H and I). These results suggest that circRAD54L2 functions as a sponge of the miR-888 family members.

miR-888 family inhibits breast cancer progression by targeting *Pdk1* mRNA.

It has been well established that miRNAs regulate their target mRNA post-transcriptionally via sequence-guided recognition. According to TargetScan (http://www.targetscan.org/) and miRanda predictions, the three prime untranslated region (3′-UTR) of *Pdk1* harbor hsa-miR-888, hsa-miR-890, hsa-miR-892a, and hsa-miR-892b binding sites (Fig. 5A). Expectedly, Real-time qPCR analysis shows that hsa-miR-888, hsa-miR-890, hsa-miR-892a, and hsa-miR-892b mimics (Supp. Fig. 2A) or inhibitors (Supp. Fig. 2B) could suppress or elevate the *Pdk1* mRNA level, respectively, in MDA-MB-231 and MDA-MB-468 cells. Consistent with mRNA level, western blot assays demonstrated hsa-miR-888, hsa-miR-890, hsa-miR-892a, and hsa-miR-892b mimics (Fig. 5B) or inhibitors (Fig. 5C) could suppress or promote the protein expression of PDK1, respectively, in MDA-MB-231 and MDA-MB-468 cells. Next, to verify this interaction, luciferase reporter vectors with the WT or MUT PDK1 3' UTR binding site were constructed. As shown in Fig. 5D, transfection of hsa-miR-888, hsa-miR-890, hsa-miR-892a, and hsa-miR-892b mimics could strongly reduce the activity of a luciferase reporter carrying the WT *Pdk1* 3′-UTR. However, the mutated luciferase reporter activity was unaffected by co-transfection with hsa-miR-888 family member mimics (Fig. 5D). These results suggest that hsa-miR-888 family members regulate PDK1 by direct interaction with *Pdk1* mRNA.

CircRAD54L2 acts as a ceRNA to regulate PDK1

The rescue experiments were designed and performed to validate whether circRAD54L2 sponges the hsa-miR-888 family members and liberates the expression of its downstream target. CircRAD54L2 knockdown decreased *Pdk1* mRNA level (Fig. 6A) and protein expression (Fig. 6B). Transfection with hsa-miR-888, hsa-miR-890, hsa-miR-892a, and hsa-miR-892b inhibitors rescued this decrease in MDA-MB-231 and MDA-MB-468 cells (Fig. 6A and B), which indicates that circRAD54L2 sponges hsa-miR-888 family members to regulate PDK1 expression in breast cancer cells. Furthermore, transduction of sh-circRAD54L2 significantly suppressed the migration and invasion, while overexpression of hsa-miR-888 family members inhibitor mix rescued migration and invasion suppression in

MDA-MB-231 and MDA-MB-468 cells (Figs. 6C). These results reveal that circRAD54L2 can significantly promote the migration and invasion of breast cancer cells by targeting the hsa-miR-888 family. Taken together, the high expression of circRAD54L2 in breast cancer demonstrates that circRAD54L2 is a proto-oncogene, sponging miR-888 family to mediate the breast cancer progression through PDK1 (Fig. 6D).

Discussion

Recently, with the development of bioinformatics and the advent of next-generation sequencing technologies [11, 15], numerous circular RNAs have been identified and studied, spanning various species. Many highly stable circRNAs are abundantly expressed, and circRNA research has been a hot topic in many diseases, especially in malignant tumor research [16-18]. Due to the abundance, stability, and the potential number of MREs they contain, circRNAs have been previously characterized could act as a miRNA “sponge” to decrease the number of miRNAs as vital factors in breast cancer [19, 20]. We demonstrated that circRAD54L2 might act as a prognostic biomarker and therapeutic target for breast cancer. Our further studies also revealed that circRAD54L2 exerts its regulatory functions through harboring miR-888 family members to rescue the expression of PDK1. These studies show that the primary function of circRNAs is to deregulate miRNAs in pathogenic processes, demonstrating their potential role in TNBC. It is vital to be served as valuable clinical prognostic biomarkers and therapeutic targets.

In conclusion, our results showed that circRAD54L2 could regulate PDK1 expression by sponging miR-888s competing for the ceRNA mechanism, indicating that circRAD54L2 may act as an essential upstream component of the regulatory circuit and providing further mechanistic evidence to support the notion that circRAD54L2/miR-888s/PDK1 is a promising therapeutic target of breast cancer.

Supplementary Material

Refer to Web version on PubMed Central for supplementary material.

Funding:

This study was supported by a grant from the Wenzhou Science&Technology Bureau (Y20180089); This work was supported by NIH/NIMHD Accelerating Excellence in Translational Science Pilot Grants G0814C01 (Q. Hao). NIH/NCI 1U54CA14393, NIH/NIMHD U54MD007598, Department of Defense Breast Cancer Research Program Grant BC043180, and NIH/NCATS CTSI UL1TR000124 (J.V. Vadgama).

Reference:

[1]. Alkabban FM, Ferguson T, Breast Cancer, StatPearls, Treasure Island (FL), 2021.

[2]. Tsang JYS, Tse GM, Molecular Classification of Breast Cancer, Advances in anatomic pathology 27(1) (2020) 27–35. [PubMed: 31045583]

[3]. Badve S, Dabbs DJ, Schnitt SJ, Baehner FL, Decker T, Eusebi V, Fox SB, Ichihara S, Jacquemier J, Lakhani SR, Palacios J, Rakha EA, Richardson AL, Schmitt FC, Tan PH, Tse GM, Weigelt B, Ellis IO, Reis-Filho JS, Basal-like and triple-negative breast cancers: a critical review with an emphasis on the implications for pathologists and oncologists, Modern pathology : an official journal of the United States and Canadian Academy of Pathology, Inc 24(2) (2011) 157–67. [PubMed: 21076464]

[4]. Vo JN, Cieslik M, Zhang Y, Shukla S, Xiao L, Zhang Y, Wu YM, Dhanasekaran SM, Engelke CG, Cao X, Robinson DR, Nesvizhskii AI, Chinnaiyan AM, The Landscape of Circular RNA in Cancer, Cell 176(4) (2019) 869–881 e13. [PubMed: 30735636]

[5]. Zheng LL, Li JH, Wu J, Sun WJ, Liu S, Wang ZL, Zhou H, Yang JH, Qu LH, deepBase v2.0: identification, expression, evolution and function of small RNAs, LncRNAs and circular RNAs from deep-sequencing data, Nucleic Acids Res 44(D1) (2016) D196–202. [PubMed: 26590255]

[6]. Liu J, Liu T, Wang X, He A, Circles reshaping the RNA world: from waste to treasure, Mol Cancer 16(1) (2017) 58. [PubMed: 28279183]

[7]. Han B, Chao J, Yao H, Circular RNA and its mechanisms in disease: From the bench to the clinic, Pharmacol Ther 187 (2018) 31–44. [PubMed: 29406246]

[8]. Rybak-Wolf A, Stottmeister C, Glazar P, Jens M, Pino N, Giusti S, Hanan M, Behm M, Bartok O, Ashwal-Fluss R, Herzog M, Schreyer L, Papavasileiou P, Ivanov A, Ohman M, Refojo D, Kadener S, Rajewsky N, Circular RNAs in the Mammalian Brain Are Highly Abundant, Conserved, and Dynamically Expressed, Mol Cell 58(5) (2015) 870–85. [PubMed: 25921068]

[9]. Salzman J, Chen RE, Olsen MN, Wang PL, Brown PO, Cell-type specific features of circular RNA expression, PLoS Genet 9(9) (2013) e1003777. [PubMed: 24039610]

[10]. Kristensen LS, Hansen TB, Veno MT, Kjems J, Circular RNAs in cancer: opportunities and challenges in the field, Oncogene 37(5) (2018) 555–565. [PubMed: 28991235]

[11]. Meng S, Zhou H, Feng Z, Xu Z, Tang Y, Li P, Wu M, CircRNA: functions and properties of a novel potential biomarker for cancer, Mol Cancer 16(1) (2017) 94. [PubMed: 28535767]

[12]. Li Y, Zheng F, Xiao X, Xie F, Tao D, Huang C, Liu D, Wang M, Wang L, Zeng F, Jiang G, CircHIPK3 sponges miR-558 to suppress heparanase expression in bladder cancer cells, EMBO Rep 18(9) (2017) 1646–1659. [PubMed: 28794202]

[13]. Hansen TB, Jensen TI, Clausen BH, Bramsen JB, Finsen B, Damgaard CK, Kjems J, Natural RNA circles function as efficient microRNA sponges, Nature 495(7441) (2013) 384–8. [PubMed: 23446346]

[14]. Glazar P, Papavasileiou P, Rajewsky N, circBase: a database for circular RNAs, RNA 20(11) (2014) 1666–70. [PubMed: 25234927]

[15]. Szabo L, Salzman J, Detecting circular RNAs: bioinformatic and experimental challenges, Nat Rev Genet 17(11) (2016) 679–692. [PubMed: 27739534]

[16]. Goodall GJ, Wickramasinghe VO, RNA in cancer, Nat Rev Cancer 21(1) (2021) 22–36. [PubMed: 33082563]

[17]. Lei M, Zheng G, Ning Q, Zheng J, Dong D, Translation and functional roles of circular RNAs in human cancer, Mol Cancer 19(1) (2020) 30. [PubMed: 32059672]

[18]. Li J, Sun D, Pu W, Wang J, Peng Y, Circular RNAs in Cancer: Biogenesis, Function, and Clinical Significance, Trends Cancer 6(4) (2020) 319–336. [PubMed: 32209446]

[19]. Yu Y, Zheng W, Ji C, Wang X, Chen M, Hua K, Deng X, Fang L, Tumor-Derived circRNAs as Circulating Biomarkers for Breast Cancer, Front Pharmacol 13 (2022) 811856. [PubMed: 35242035]

[20]. Zhou X, Jian W, Luo Q, Zheng W, Deng X, Wang X, Borkhuu O, Ji C, Li D, Fang L, Circular RNA_0006014 promotes breast cancer progression through sponging miR-885-3p to regulate NTRK2 and PIK3/AKT pathway, Aging (Albany NY) 14(undefined) (2022).

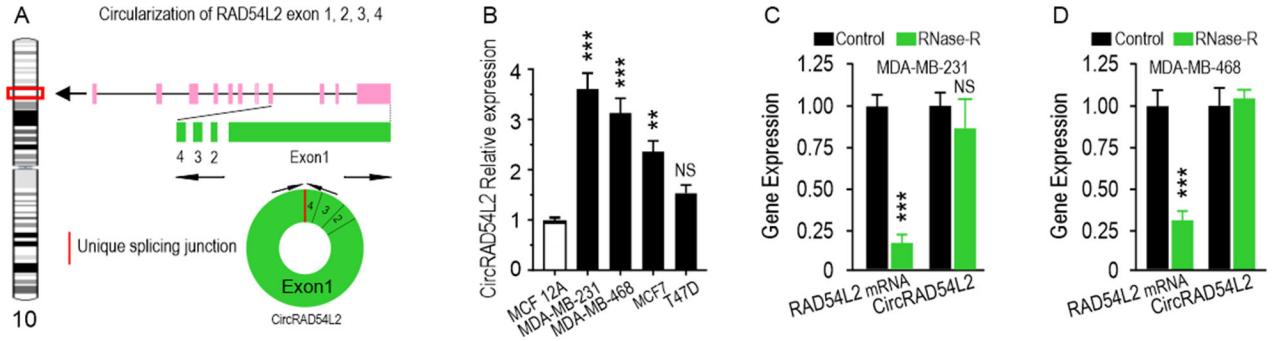

Fig. 1. CircRAD54L2 is upregulated in TNBC cell lines.

A. Schematic illustration showing the circularization of RAD54L2 exon 1, 2, 3, 4 forming circRAD54L2. The red arrow indicates the unique splicing junction of circRAD54L2. B. The expression of circRAD54L2 in TNBC cell lines is significantly higher than in non-tumor breast cell lines. C. RT-qPCR analysis of circRAD54L2 and RAD54L2 transcripts in the presence or absence of RNase R treatment in MDA-MB-231 and MDA-MB-468 (D) cells. (**p < 0.01; ***P < 0.005; NS, Not Significant).

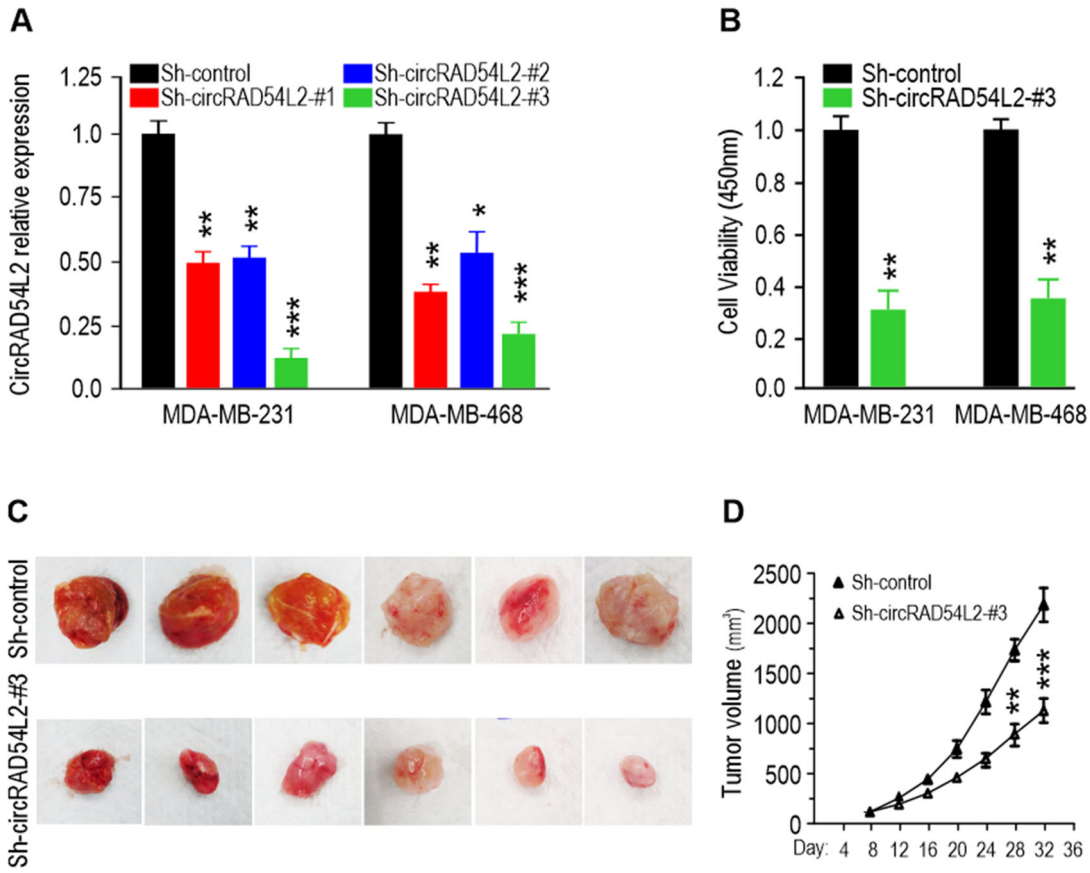

Fig. 2. Knockdown of circRAD54L2 inhibits breast cancer growth.

A. ShRNAs were used to silence circRAD54L2 expression, and sh-circRAD54L2-#3 has the strongest inhibitory effect in MDA-MB-231 and MDA-MB-468 cells. B. MTS assay to detect cell viability in MDA-MB-231 and MDA-MB-468 cells. C. Xenograft assay with MDA-MB-231 cells stably knockdown circRAD54L2. D. Knockdown of circRAD54L2 decreased the volume of the MDA-MB-231 xenograft tumors. (*p <0.05; **p < 0.01; ***P < 0.005).

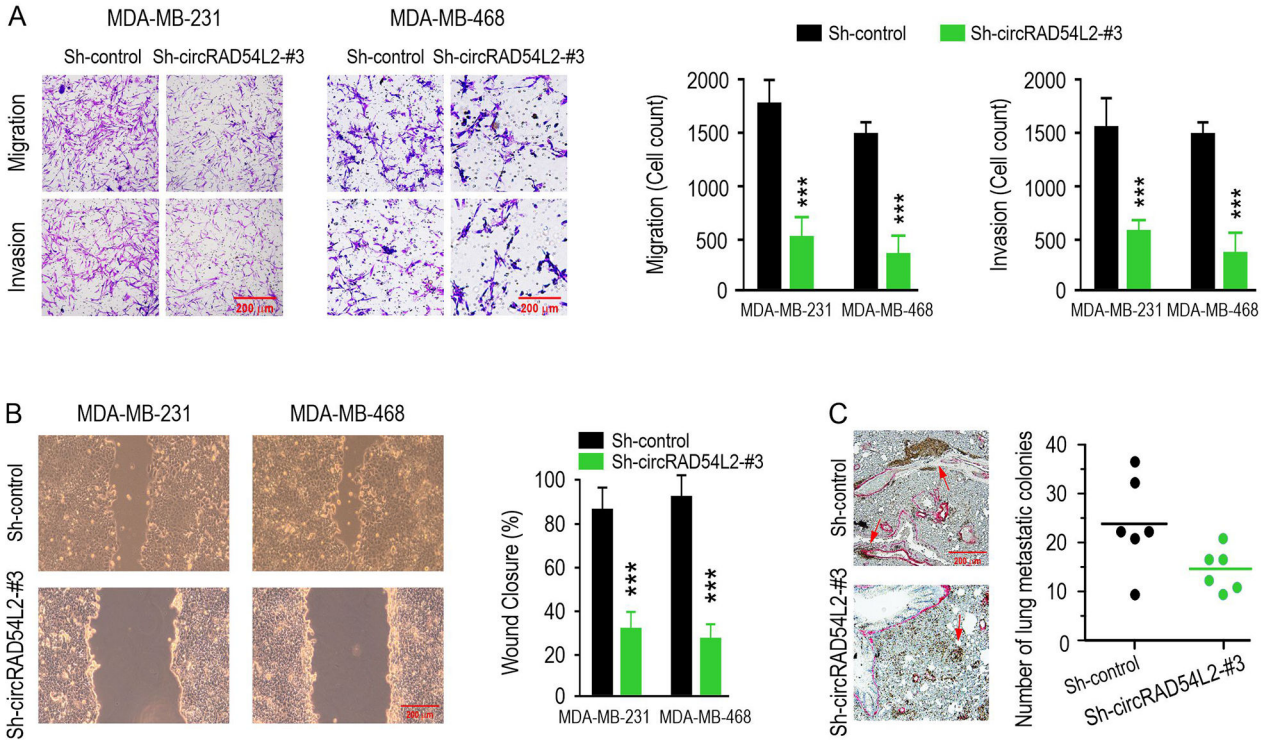

Fig. 3. Knockdown of circRAD54L2 inhibits breast cancer cells migration and invasion *in vitro* and tumor metastasis *in vivo*.

A. Silencing circRAD54L2 inhibits the migration and invasion of MDA-MB-231 and MDA-MB-468 cells by transduction with sh-circRAD54L2. Right panel: Quantification of migration and invasion. B. Wound healing assay to evaluate the cell migration capability of sh-circRAD54L2 in MDA-MB-231 and MDA-MB-468 cells. Right panel: Quantification of migration. C. Representative images of lung metastatic colonies stained by hematoxylin in two treatment groups (n=6 in each group). Lung metastatic foci were counted microscopically. Arrowheads indicate metastatic colonies. Right panel: Number of metastatic lung colonies. (*p <0.05, **p < 0.01, ***P < 0.005).

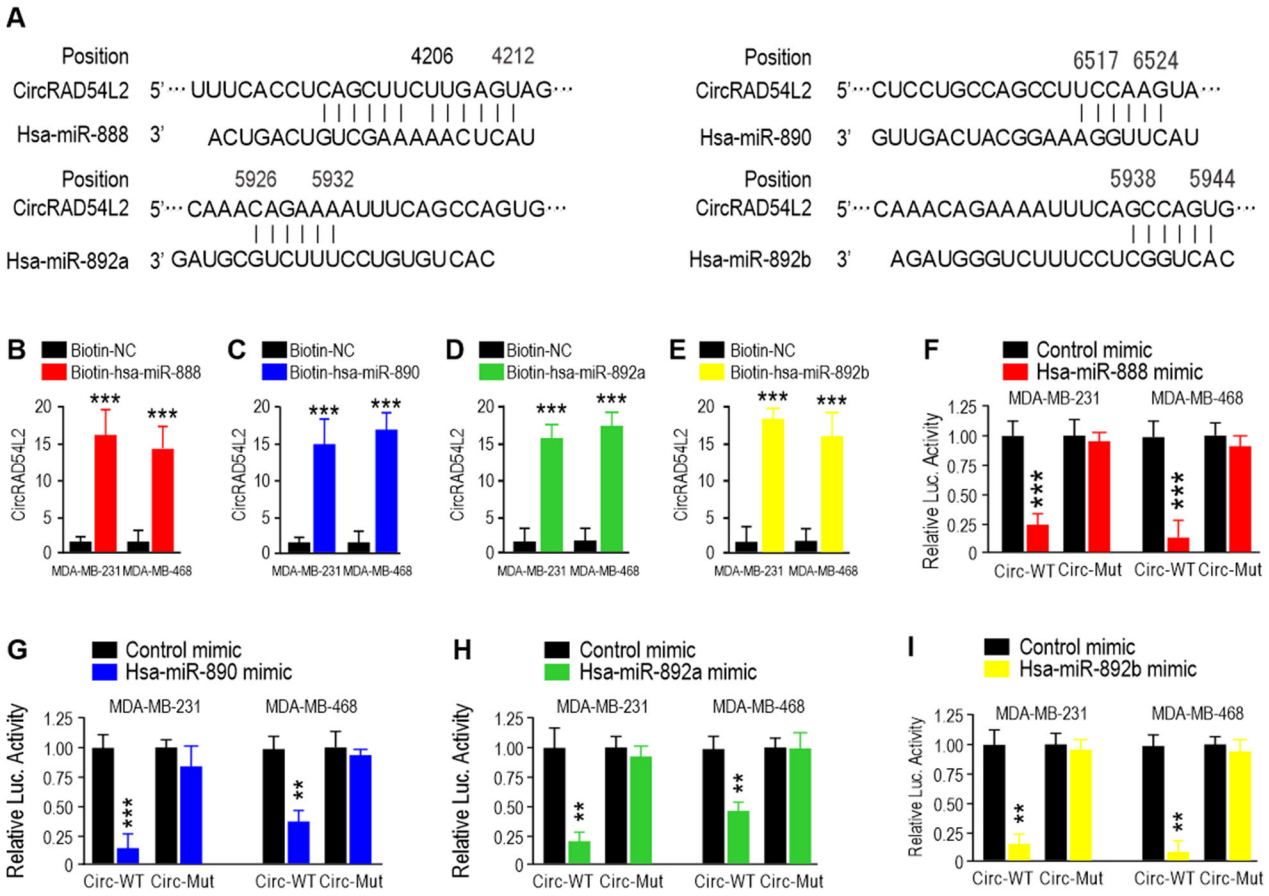

Fig. 4. CircRAD54L2 acts as a sponge for the hsa-miR-888 family in breast cancer cells.

A. The predicted binding sites of hsa-miR-888, hsa-miR-890, hsa-miR-892a, and hsa-miR-892b within the circRAD54L2. B. The biotinylated hsa-miR-888, hsa-miR-890 (C), hsa-miR-892a (D), and hsa-miR-892b (E) were transfected into MDA-MB-231 and MDA-MB-468 cells. After streptavidin capture, circRAD54L2 levels were quantified by qRT-PCR. F. Luciferase reporter assay was used to confirm the interaction between circRAD54L2 and hsa-miR-888, hsa-miR-890 (G), hsa-miR-892a (H) and hsa-miR-892b (I). (*p <0.05, **p < 0.01, ***P < 0.005).

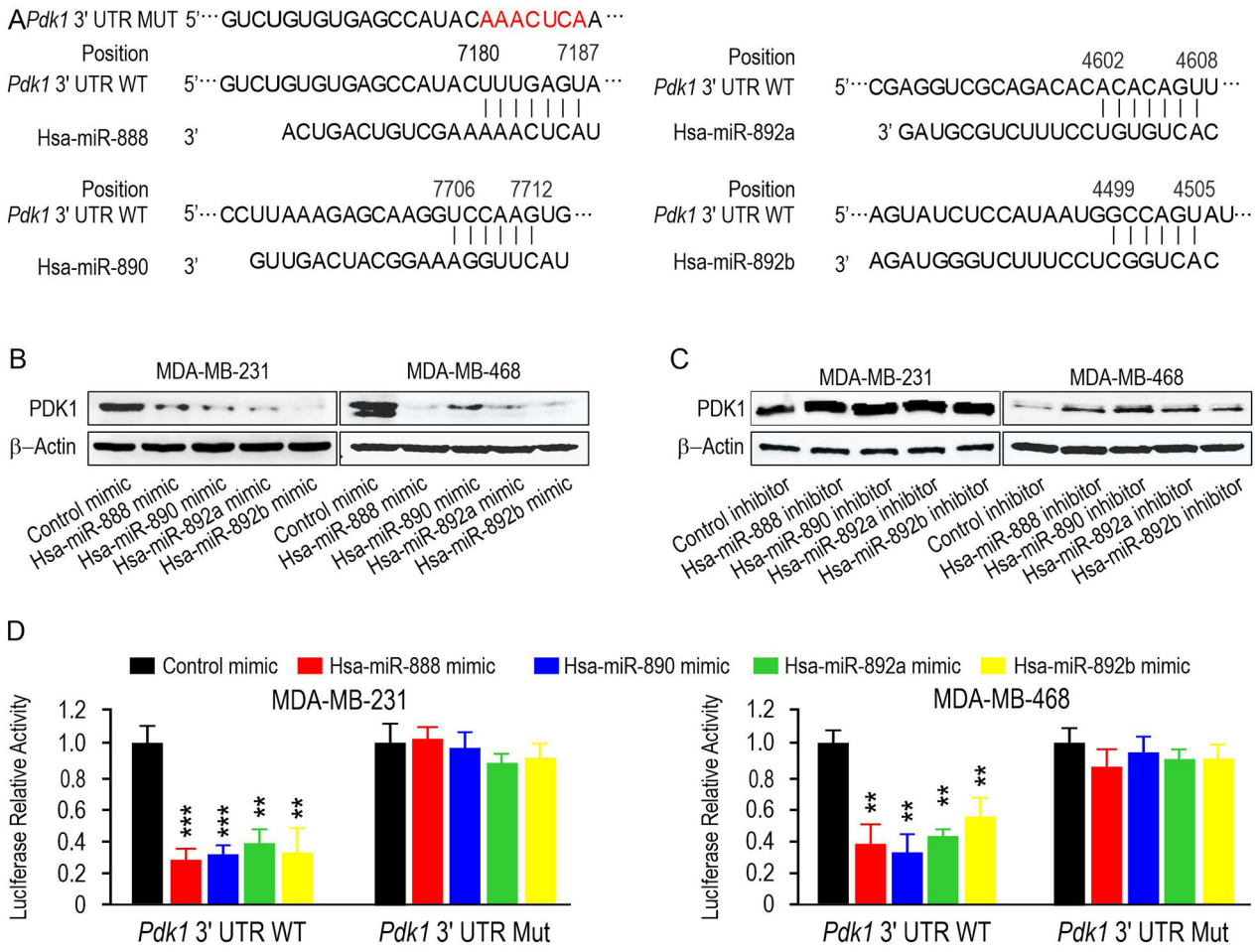

Fig. 5. miR-888 family inhibits breast cancer progression through targeting *Pdk1* mRNA.

A. Predicted miR-888 family binding sites in the 3′-UTR of *Pdk1* mRNA. B. miR-888 family member mimics or inhibitors (C) decreased or increased the protein expression level of PDK1 in MDA-MB-231, and MDA-MB-468 cells. D. Luciferase reporter assay was used to confirm the interaction between *Pdk1* mRNA and miR-888 family members in MDA-MB-231 and MDA-MB-468 cells. (*p <0.05, **p < 0.01, ***P < 0.005).

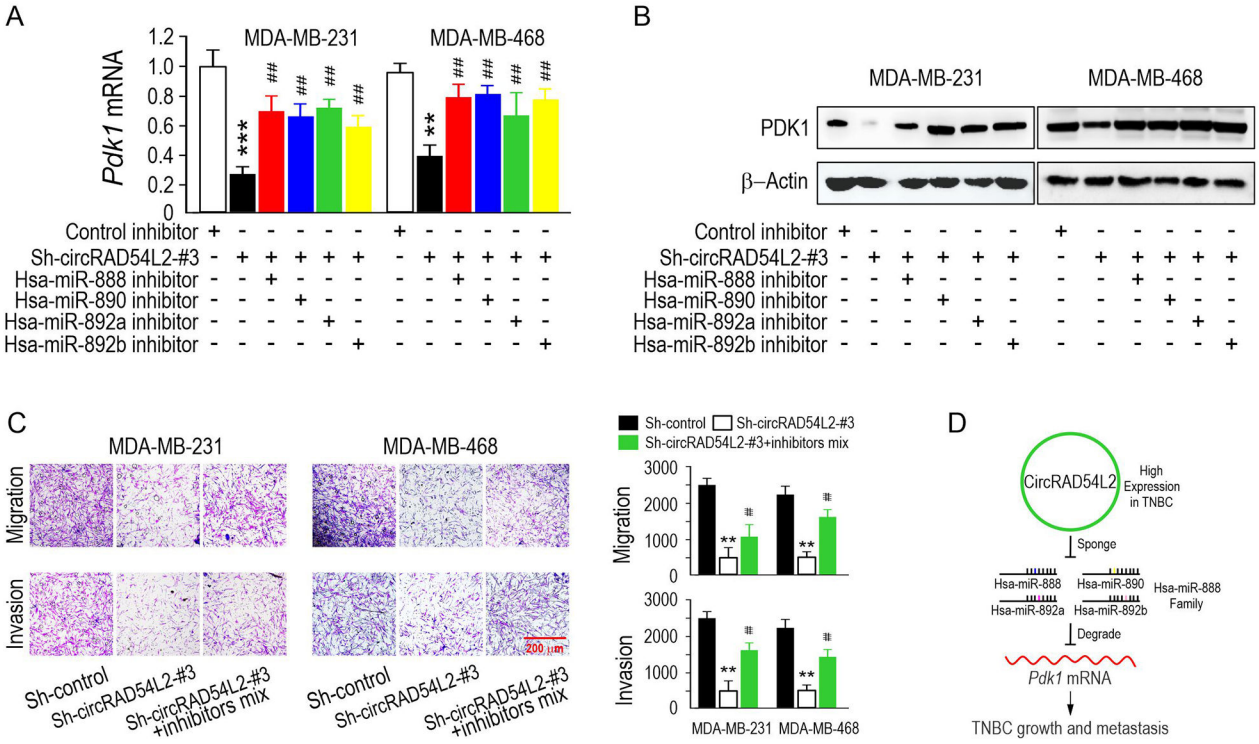

Fig. 6. CircRAD54L2 regulates PDK1 expression and inhibits breast cancer progression via targeting the miR-888 family.

A. qRT-PCR and Western blot analysis (B) showed that miR-888 family inhibitors rescued circRAD54L2 caused *Pdk1* mRNA and protein (B) decrease in MDA-MB-231 and MDA-MB-468 cells. C. Transwell migration and invasion assays demonstrated that miR-888 family member inhibitors mix rescued sh-circRAD54L2 decreased the migration and invasion capability in MDA-MB-231 and MDA-MB-468 cells. Right panel: Quantification of migration and invasion. D. Function and mechanism of circRAD54L2 during breast cancer progression. (**p < 0.01; ***P < 0.005; ## p < 0.01 compared with miR-888 family)